

Chapter 22

Single-Molecule Conductance Theory Using Different Orbitals for Different Spins: Applications to π -Electrons in Graphene Molecules



Anatoliy V. Luzanov

Abbreviations

AO	Atomic orbital
DODS	Different orbitals for different spins
EHF	Extended Hartree-Fock
FCI	Full configuration interaction
GF	Green's function
GQD	Graphene quantum dot
HPHF	Half-projected Hartree-Fock
MO	Molecular orbital
MSE	Molecular-scale electronics
QCLRI	Quasi-correlated long-range interaction
QCTB	Quasi-correlated tight-binding (model)
RHF	Restricted Hartree-Fock
TB	Tight-binding (model)
UHF	Unrestricted Hartree-Fock
WBL	Wide-band limit

22.1 Introduction

The emergence of molecular-scale electronics (MSE) opened a remarkable vista for quantum science and nanoscale devices. Over the past two decades the various mechanisms of molecular conductance have been proposed and studied from many

A. V. Luzanov (✉)

SSI "Institute of Single Crystals", NAS of Ukraine, Kharkiv, Ukraine

angles at the experimental and theoretical levels [1–6]. However, some vital issues remain to be fully clarified, and the influence of many-body effects is one of them. Indeed, much theoretical work was done, seemingly successfully, on simple range models, like one-electron tight-binding (TB) approximation (see, e.g., Refs. [6–12]). At the same time, many studies have been reported on the use of more reliable approaches which include electron correlation effects (Refs. [13–19]. and many others). However, high-level many-electron models are too demanding, especially for the MSE applications, so that even simple TB theories retain their certain usefulness.

In this paper we give the new results of using the modified approach of TB type which quite recently was applied in the MSE context [20]. This is the quasi-correlated tight-binding (QCTB) approximation developed in Refs. [21–23]. Actually QCTB is closely related to one old model first discussed in Ref. [24] for spin-doublet alternant π -radicals. Really, QCTB is but a simplest implementation of the different orbitals for different spins (DODS) approach. Nevertheless, in case of alternant π -conjugated hydrocarbons, or bipartites (in graph theoretic terms), QCTB can mimic, more or less crudely, π -electron correlation effects, particularly electron unpairing in molecular closed shells [22, 23]. Interestingly, QCTB was also adopted in Ref. [25] for analyzing fine effects of “spin repulsion” in bipartite networks.

One of the aims of the present paper is to check the predictions of TB and QCTB against the “exact” π -electron results of the full configuration interaction (FCI) method for small π -systems. For moderate-size conjugated structures, such as graphene nanoflakes (for which FCI cannot be undertaken), we additionally propose to use the more advanced DODS model due to Smeyers [26], that is, the half-projected Hartree-Fock (HHPF) method. The latter is the well-known and well-elaborated electron-correlation model (see, e.g., Refs. [26–30].), but it has not been employed previously for MSE problems. On this account, a number of formal points, e.g., the GF method for HHPF, required clarification. In the paper the abovementioned issues are discussed in detail.

The layout of the present work is as follows. The next section contains the main definitions and prerequisite facts about one-electron theory of molecular conductance. Section 22.3 addresses the QCTB machinery and derivation of the working equations for the corresponding one-electron Green’s function (GF). Section 22.4, along with Appendix A, develops the basic expressions of HHPF approach as they are related to the problem. In Sect. 22.5, we study electron conductance in various graphene structures, and in the last section we summarize the results, outlining perspectives for future work. Several supporting topics and details are addressed in Appendices.

22.2 Simple One-Electron Schemes

Let us begin with the main definitions and notations which are typical for the single-molecule electron transport theory. As in most current computations of molecular conductance, we will assume a ballistic (without scattering) electron transport. We consider, in a conventionally simplified manner, the coherent transport

through a conjugated molecule sandwiched between two leads (contacts). The leads which are attached to atoms a and b of the given molecule are characterized by phenomenological broadening parameters Γ_a and Γ_b . Such a contact pair will be named the (a,b) connection. Then within the wide-band limit (WBL) approximation (see [31] and references therein) a working formula for the corresponding molecular conductance, g_{ab} , is

$$g_{ab}/g_0 = \Gamma_a \Gamma_b |G_{ab}|^2. \quad (22.1)$$

Here g_0 is the quantum conductance unit (in atomic units, $g_0 = \pi^{-1}$); G_{ab} symbolize a relevant matrix elements of the effective retarded one-electron GF, G , for the molecule under study. In general, G depends on real-energy argument E (an incoming electron energy). Moreover, G must take into account effects of coupling between molecular wire and leads.

In one-electron (mean-field) approximation, G can be taken as a resolvent of the appropriate effective Hamiltonian h . If we ignore broadening of molecular energy levels due to their interaction with the leads, then we can set $G(E) = R(E)$ where the standard resolvent matrix R is of the form

$$R(E) = (E + i0^+ - h)^{-1}. \quad (22.2)$$

Here and throughout the paper, any number in matrix expression is understood as a scalar diagonal matrix; e.g., $E \equiv EI$, with I being the identity matrix of respective size. We will also often omit E in $R(E)$ and $G(E)$; e.g., $G \equiv G(E)$. Generally, G as an effective molecular GF differs from R owing to the abovementioned coupling effects with the leads.

We start with the conventional π -electron TB approximation, i.e., we will work now with the Hückel method and its extensions. The Hückel Hamiltonian matrix is well known, and in the next section we will discuss it for bipartites in greater detail. The essential part of the currently used molecular conductance theories is an explicit inclusion of the broadening effect in the effective G . If the WBL prescription is applied, then instead of Eq. (22.2), we can express GF in one-electron approximation as follows:

$$G(E) = (E + i \Gamma^{[a,b]} - h)^{-1}, \quad (22.3)$$

with $\Gamma^{[a,b]}$ being a broadening matrix. The latter is predominately localized on atoms a and b coupled with the leads, so within π -electron schemes we have explicitly

$$\Gamma^{[a,b]} = (\Gamma_a |a\rangle \langle a| + \Gamma_b |b\rangle \langle b|) / 2, \quad (22.4)$$

where Dirac kets $|a\rangle$ and $|b\rangle$ are the $2p\pi$ atomic orbitals (AOs) of the carbon atoms involved into the studied (a,b) connection (e.g., see, Ref. [32]).

22.3 QCTB Model for Effective Green's Functions

Before applying QCTB scheme to MSE problems, we recall first the customary TB π -electron model. The TB Hamiltonian will be denoted by h^0 . From now on we consider only plane bipartite carbon-containing networks—they must not possess odd-membered cycles (König's theorem). In reality, such systems make up a vast majority of the conjugated hydrocarbons of the MSE interest. Let us recall a common structural property of these bipartites. All sites in them can be always divided into two nonintersecting sets of starred (*) and unstarred (o) sites (in Coulson's terms), and the starred sites are chemically interbonded with the unstarred ones only. Then in the standard π -AO basis set the h^0 matrix allows the known block skew-diagonal representation:

$$h^0 = - \begin{pmatrix} 0 & B \\ B^T & 0 \end{pmatrix}, \quad (22.5)$$

where block $B \equiv (h^0)_{*o}$ describes interactions between starred and unstarred sites; superscript T denotes matrix transposition. Apart from a scaling factor $|\beta_0|$ (β_0 is a resonance integral), this B is but the adjacency matrix composed of ones for connected sites; rest elements of B are zero by definition (TB approximation). Evidently, using $h = h^0$ for GF in Eq. (22.2) is straightforward. For the given (a,b) connection, the corresponding GF will be signified by G^{TB} . Then, as in Eq. (22.3) we have.

$$G^{TB} = \left(E + i \Gamma^{[a,b]} - h^0 \right)^{-1}. \quad (22.6)$$

Now we turn to QCTB [21, 22], which is the main object of the study here. As to precursors of QCTB, see, besides the first paper [24], also Refs. [33–35], where the simplified schemes were formulated by invoking DODS and the Hubbard Hamiltonian. In QCTB [21–23] we also make using a spin-splitting description, starting with two effective TB-like Hamiltonians h^α and h^β . Thus, we define

$$h^\alpha = - \begin{pmatrix} \delta & B \\ B^T & -\delta \end{pmatrix}, \quad h^\beta = - \begin{pmatrix} -\delta & B \\ B^T & \delta \end{pmatrix}, \quad (22.7)$$

and associate these Hamiltonians with subsystems of α -electrons (with spin up) and β -electrons (with spin down), respectively. In Eq. (22.7) by parameter δ we bring in a spin polarization, thus mimicking electron correlation effects. Below δ is a fixed number.

Having now at our disposal Hamiltonians h^α and h^β we shall generate two auxiliary resolvents:

$$R^\alpha = (E + i0^+ - h^\alpha)^{-1}, \quad R^\beta = (E + i0^+ - h^\beta)^{-1}. \quad (22.8)$$

For spin-singlet states, a symmetrized combination should be used instead, thus giving the QCTB “resolvent” matrix, R^{QCTB} , of the form:

$$R^{\text{QCTB}} = (R^\alpha + R^\beta) / 2. \quad (22.9)$$

Clearly, this type of GFs pays no attention to the abovementioned energy-level broadening. The more consistent should be the effective Green’s function G^{QCTB} of the form

$$G^{\text{QCTB}} = \left(I / R^{\text{QCTB}} + i \Gamma^{[a,b]} \right)^{-1}, \quad (22.10)$$

which is based on a rather general expression, Eq. (27), in Ref. [14]. Evidently, $G^{\text{QCTB}} = R^{\text{QCTB}}$ if $\Gamma^{[a,b]} = 0$. For the given (a,b) connection, the thus constructed G^{QCTB} will serve as a basic approximation which provides us with a simplistic but reasonable way to describe π -electron correlation effects relevant to MSE problems. Note that in Ref. [20] we have made preliminary applications to demonstrate the possibilities of QCTB for computing molecular conductance in oligomer structures. In the cited paper, the energy-level broadening was handled using a too simplistic (scalar) approach.

22.4 Use of the Half-Projected Hartree-Fock π -Model

As we saw previously in Ref. [20], QCTB provides rather semiquantitative and frequently only qualitative results due to neglecting long-range interactions effects. In other words, in QCTB the systematic errors are incurred by using topological in their essence Hamiltonians, Eq. (22.7). On this account we must adopt more general DODS models for π -electrons. The best variational DODS model is Löwdin’s extended Hartree-Fock (EHF) method [36]. However, GF is too tricky to be calculated consistently at the EHF level; at least, no results in this direction are known at present. In this situation, the well-known HPHF model of Smeyers [26], as a simplified version of EHF, seems to be a reasonable alternative choice. Below, we elaborate the GF computational technique at the HPHF level.

Firstly, we briefly recall the basic points, following closely the presentation of HPHF from Refs. [26, 28]. Only singlet molecular ground states will be considered in the present paper, so we will deal with even-numbered N -electron systems where $N = 2n$ and n is an integer. Recall that for all DODS approaches, the starting point is the wave function $|\Phi^{\alpha,\beta}\rangle$ of unrestricted Hartree-Fock (UHF) type. We take this in the spin-free form:

$$|\Phi^{\alpha,\beta}\rangle = |\Phi^\alpha\rangle \otimes |\Phi^\beta\rangle, \quad (22.11)$$

where vectors $|\Phi^\alpha\rangle$ and $|\Phi^\beta\rangle$ are spin-free determinants. The latter are built up from the given spin-free MOs,

$$\left\{ \left| \phi_i^\alpha \right\rangle \right\}_{1 \leq i \leq n}, \quad \left\{ \left| \phi_i^\beta \right\rangle \right\}_{1 \leq i \leq n} \quad (22.12)$$

for spin-up and spin-down electrons, respectively. Of course, Eq. (22.11) is equivalent to the usual unrestricted Slater determinant; the above spin-free representation is merely more convenient for manipulations and corresponds to the classical Waller-Hartree double-determinant method [37].

As is well known, generally the UHF wavefunction $|\Phi^{\alpha,\beta}\rangle$ is a non-spin-pure state. In order to recover a spin-pure or nearly spin-pure state, an appropriate spin projection should be performed. The simplest symmetrization of spin-up and spin-down electrons is such an approximate projection procedure for spin-singlet states. This is precisely used in HPHF, thus giving the improved wave function

$$\left| \Psi^{\text{HPHF}} \right\rangle = \left| \Phi^{\alpha,\beta} \right\rangle + \left| \Phi^{\beta,\alpha} \right\rangle. \quad (22.13)$$

The variational HPHF equations for MO sets, Eq. (22.12), related to state vector (22.13) are not so difficult to derive [26–28], and hence we omit them for brevity.

Now turn to ionized states which are needed for constructing GF. Following Ref. [28], we consider $(2n-1)$ -electron state vector $|\Psi_+^{\text{HPHF}}\rangle$. It is obtained from $|\Psi^{\text{HPHF}}\rangle$ by removing one electron described by own MO $|\phi\rangle$ which we must determine variationally. Namely, let us introduce two $(n-1)$ -electron states, $|\Phi_+^\alpha\rangle$ and $|\Phi_+^\beta\rangle$, where explicitly $|\Phi_+^\alpha\rangle = \sqrt{n} \langle \phi(n) | \Phi^\alpha \rangle_{(n)}$ and likewise for $|\Phi_+^\beta\rangle$. These states correspond to electron annihilation in $|\Phi^\alpha\rangle$ and $|\Phi^\beta\rangle$, respectively. Then, the approximate spin-doublet state vector is

$$\left| \Psi_+^{\text{HPHF}} \right\rangle = \left| \Phi_+^\alpha \right\rangle \otimes \left| \Phi^\beta \right\rangle + \left| \Phi^\alpha \right\rangle \otimes \left| \Phi_+^\beta \right\rangle. \quad (22.14)$$

The variational equation for $|\phi\rangle$ that optimizes the energy of this ionized state is presented in Ref. [28]. Based on it, we have derived in Appendix A the relations required for R^{HPHF} (GF without broadening effects). Once having computed R^{HPHF} from Eqs. (22.A2), (22.A8), and (22.A9), we evaluate the full GF matrix, G^{HPHF} , by adding broadening effects in the same manner as in Eq. (22.10):

$$G^{\text{HPHF}} = \left(I / R^{\text{HPHF}} + i \Gamma^{[a,b]} \right)^{-1}. \quad (22.15)$$

The quality of this HPHF model for GF is estimated for aromatic structures in Appendix B. In the latter we show that for the small cyclic molecules treated by the standard π -electron theory, the HPHF results for GF (at $E = E_F$ where E_F is the Fermi energy) are close to FCI quality (Table 22.3). In the same table, QCTB demonstrates a reasonable behavior, but not as good as HPHF. Nevertheless, QCTB

is systematically better than TB, and it is in agreement with our previous study of polyenic systems [20].

One deficient feature of HPHF is a lack of size-consistency (for a general consideration of this and related issues see review [38]). We discuss the issue for GF in detail in Appendix B, and show that in practice this deficiency is not too severe for small and middle-size systems. It allows us, for the similar systems, to consider the obtained HPHF results as giving realistic estimations of GF matrix elements. At least, the HPHF data are much more favorable than other ones which are produced for graphene molecules by TB and even the restricted Hartree-Fock (RHF) method. In fact, we will employ HPHF as a tool for the quality assessment of low-level models (QCTB and TB) in middle-size graphene molecules.

22.5 Applications to Graphene Molecules

22.5.1 Small Graphene Molecules

The graphene networks are often regarded as promising candidates for designing MSE materials. In this context a variety of approximations was made to estimate electronic and conductance properties of nanographene molecules (Refs. [8, 39–45], and others). The π -electronic structure of several relatively small graphene quantum dots (GQDs) is also investigated in Refs. [46, 47].

In the present calculations of the effective GF and conductance spectra, we employ broadening parameter $\Gamma = \Gamma_a = \Gamma_b = 0.1$ eV taken from Ref. [18]. In all the plots we show conductance (in the g_0 units) as a function of electron energy E . In the abscissa, E is in eV, and E_F , is shifted to 0 for convenience. Moreover, we make use of the logarithmic ordinate. The conductance spectra are plotted for the various π -models in this way: HPHF in red, QCTB in green, and TB in black dashed. We will also signify by R_0 the GF matrix elements at $E = E_F$.

We start our investigation with studying two small graphene molecules shown on Fig. 22.1. The first one is GQD-56 (in our notations here) which is the 56 carbon-atom circumpentacene molecule. It has been examined in a number of works [8, 39, 40] as an interesting example of the graph-theoretic (within TB) conductance theory. The second is GQD-62, that is a 62 carbon-atom structure as a particular example of an armchair graphene nanoflake studied in Ref. [44]. In Table 22.1 we

Fig. 22.1 Structure of GQD-56 and GQD-62 and the studied connections. The sites (colored disks) which are attached to electrodes are connected each other by conditional dashed lines

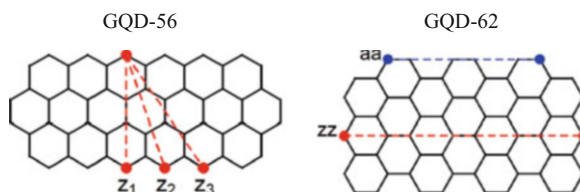


Table 22.1 GF matrix elements R_0 ($E = E_F$) for contact pairs \mathbf{z}_1 , \mathbf{z}_2 , and \mathbf{z}_3 in GQD-56, and for pairs \mathbf{aa} and \mathbf{zz} in GQD-62, accordingly to Fig. 22.1

Contact pair	R_0^{HPHF}	R_0^{QCTB}	R_0^{RHF}	R_0^{TB}
\mathbf{z}_1	-0.246	-0.281	-0.719	$-67/42 \cong -1.595$
\mathbf{z}_2	0.131	0.132	0.579	$50/21 \cong 2.381$
\mathbf{z}_3	-0.036	-0.013	-0.337	$-55/21 \cong -2.619$
\mathbf{aa}	0.020	0.042	0.012	$16/2037 \cong 0.008$
\mathbf{zz}	-0.155	-0.108	-0.175	$-625/679 \cong -0.921$

give a small piece of information related to the selected connections in GQD-56 and GQD-62 (for GQD-56, the same contact pairs are studied in Refs. [8, 39, 40].).

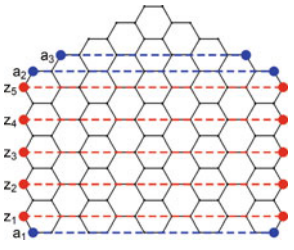
As seen from Table 22.1, TB predicts, too large GF elements in GQD-56, particularly for relatively distant connections in zigzag-type contact pairs (denoted by \mathbf{z}_j and shown by red dashed lines in the table). More than that, within TB, the matrix elements G_{ab} become spuriously larger with increasing distance between atoms a and b of the contact pair. At the same time, in the GQD-56 example as well as in many other ones, such long-distance atomic pairs have small values of usual π -bond orders (nondiagonal density matrix elements in AO basis). These bond orders, as a rule, qualitatively correlate with the corresponding G values. Such a natural fact argues additionally in favor of HPHF and QCTB but not in favor of TB. Overall, we can conclude that even small graphene molecules with zigzag edge topology require more refined tools than that based on Eq. (22.5) for the simple TB scheme.

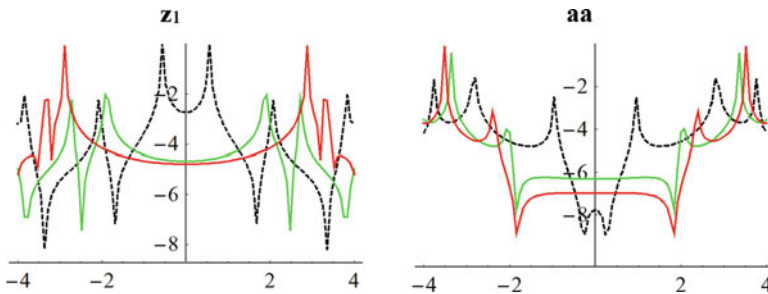
The case of GQD-62 seems somewhat different. Here we consider the GF π -electron elements for two types of long-distance connections: the zigzag connection, \mathbf{zz} , involving both sites on zigzag-type edges (red dashed line on the picture in Fig. 22.1), and the armchair connection, \mathbf{aa} , involving both sites on armchair-type edges (blue dashed line in Table 22.2). We see from Table 22.1 that in GQD-62 \mathbf{zz} connection is of the same behavior as in GQD-56, but \mathbf{aa} connection is much weaker, and this connection is less influenced by electron correlation effects, so that even TB provides a reasonable value of the corresponding GF element at E_F . These peculiarities of armchair-type connections are rather typical (see the next subsection).

On the basis of Table 22.1, we can state that the QCTB results are in a semiquantitative agreement with the more reliable HPHF data. For larger graphene molecules QCTB works less well, as will be seen from the subsequent discussion. As for the RHF model, it works only slightly better than TB. Moreover, in large conjugated π -systems, RHF suffers from the so-called Hartree-Fock instabilities (it was demonstrated in Ref. [47] for moderate-size graphene molecules). Hence, RHF can come to inappropriate broken-symmetry solutions, and for this reason we will refrain from further use of RHF for graphenes.

Consider now conductance spectra for our GQDs. In Fig. 22.2 we present them for the most efficient zigzag contact \mathbf{z}_1 in GQD-56 and for the armchair contact \mathbf{aa} in GQD-62. It is seen that even far from the Fermi level, QCTB gives satisfactory results, at least at a qualitative level, but TB does not. It means that a possible

Table 22.2 GQD-130: Comparison of GF matrix elements R_0 ($E = E_F$) for contact pairs, \mathbf{a}_j , and \mathbf{z}_j at the HPHF, QCTB, and TB levels

GQD-130 with contact pairs	Pair	R_0^{HPHF}	R_0^{QCTB}	R_0^{TB}
	\mathbf{z}_1	-0.015	-0.030	-1.784
	\mathbf{z}_2	-0.016	-0.032	-3.945
	\mathbf{z}_3	-0.011	-0.025	-3.193
	\mathbf{z}_4	-0.014	-0.025	-1.147
	\mathbf{z}_5	-0.007	-0.010	-0.129
	\mathbf{a}_1	0.003	0.003	0.001
	\mathbf{a}_2	0.005	0.010	0.001
	\mathbf{a}_3	0.030	0.072	0.030

**Fig. 22.2** Conductance spectra for connection \mathbf{z}_1 in GQD-56 and connection \mathbf{aa} in GQD-62 (see Fig. 22.1) within the HPHF (in red), QCTB (in green), and TB (in black dashed)

agreement between selected GF values of TB and more advanced models (as in the case of GF at $E = E_F$ for contacts in GQD-62) may be misleading as to a real accuracy of the low-level approach in whole.

22.5.2 Graphene Quantum Dot C_{130}

We turn to a more extended graphene structure C_{130} , further named as GQD-130, which is displayed in Table 22.2. This GQD was synthesized in Ref. [48]. The intrinsic π -electron properties of GQD-130 were considered recently in Refs. [47]. Again, we examine the GF π -electron elements of GQD-130 for two types of long-distance connections: zigzag connections, \mathbf{z}_j , and armchair connections,

\mathbf{a}_j (respectively, red and blue dashed lines on the molecule image in Table 22.2). We see from the table that there is the same, as in GQD-62, significant difference between these two types of the connections: the zigzag connections give a much greater conductance at $E = E_F$ than the armchair connections for all the models used. At the quantitative level, the calculations on zigzag channels also display a sharp difference between the non-correlated model (TB) and the correlated models (HPHF and QCTB). In GQD-130, the long-distant zigzag GF elements, being small in HPHF and QCTB, behave quite correctly—in a striking contrast to TB.

It is interesting to compare these results with those for short-distance contact pairs in the same system. For instance, a maximum absolute value, G_{\max} , of the GF matrix elements at the Fermi energy is attained on the borders—for the strongest C-C π -bonds formed by the two nearest neighbor atoms in \mathbf{z}_5 and \mathbf{a}_2 . By using HPHF, QCTB, and TB we find the corresponding G_{\max} to be equal to 0.75, 0.70, and 0.98, respectively. Thus, in all the models we obtain a reasonable value of order 1 for the GF elements of strong π -bonds, as in the ethylene molecule where $(R_0^{\text{TB}})_{1,2} = 1$. We find that in this case, and in many other sufficiently large systems with strong electron correlation, TB gives sensible results only for too closely situated leads, whereas QCTB widely agrees with HPHF, but mainly in qualitative terms, if including all long-distance connections.

For completeness, in Fig. 22.3 we plotted the conductance spectra for the most interesting long-distance connections in GQD-130. Restricting to a small energy domain (say, to the interval $[-2 \text{ eV}, 2 \text{ eV}]$ in the abscissa), we observe that indeed QCTB is fairly good for the more efficient zigzag-type channel, but QCTB is only semiquantitatively acceptable for the weak armchair-type channel. As expected, for the same nanographene problem, the TB plots turn out to be entirely wrong quantitatively as well as qualitatively. At last, our experience with HPHF and QCTB tells that the conductance spectra of other graphene-like molecules with large zigzag edges are fairly similar to that of GQD-130.

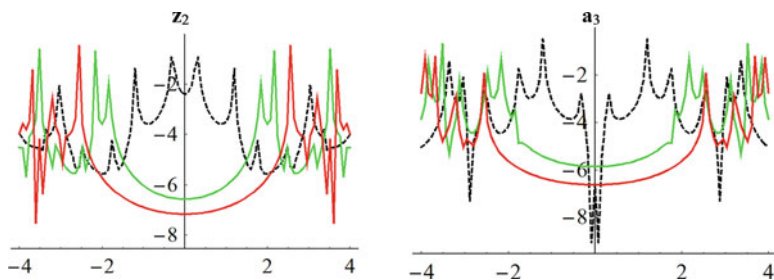


Fig. 22.3 Conductance spectra of GQD-130 for connections \mathbf{z}_2 (left panel) and \mathbf{a}_3 (right panel) within HPHF (red), QCTB (green), and TB (black dashed)

22.6 Conclusion

A large part of current theoretical studies of single-molecule conductance suggests a soundness of simple tight-binding (TB) π -schemes (at least in qualitative terms). However, as could be expected, the TB approach is too crude for MSE. Hence, it was practically important to scrutinize TB more rigorously and determine its actual validity for computing π -electron Green's functions. In this context, particularly important is the appropriate analysis of nanostructural classes, such as graphene-like molecules. Here we examined some representative graphenic molecules, thus continuing preliminary investigations in Ref. [20]. In the cited work, TB for GF was improved in an unsophisticated manner by invoking QCTB model [21, 22]. In turn, this has caused the need to examine QCTB per se, especially for sufficiently large systems. For this aim we have now brought into play a helpful HPHF model allowing study of extended systems at an affordable cost.

Specific computations on nanographenes corroborate the qualitative (but rarely quantitative) usefulness of QCTB and its ability to provide us with a more adequate physical picture than TB does. More than that, dealing with conductance spectra at the TB level turns out to be meaningless, particularly, for long-distant contact pairs in nanographenes, and it seems to apply to any extended conjugated π -system. Yet, the fact that simple TB schemes are not adequate to treat MSE for large π -structures even qualitatively, was not generally recognized, and we believe that the results reported here will help to draw a serious attention to a more realistic assessment of the TB model.

As usual, many unresolved issues remain. Specifically, there is a nontrivial problem how to improve HPHF by constructing a not too complicated scheme with a better account for electron correlation in large-scale systems. In this issue, McWeeny's generalized product functions [49] can be used for a modeled molecular composite derived from the system in question by dividing it into weakly interacting (localized) fragments. We believe that the McWeeny approach may be able to alleviate the size-inconsistency problem in HPHF. At the same time it seems sensible to explore in detail another our DODS-like approach proposed here in Appendix B as a quasi-correlated long-range interaction (QCLRI) model. There are encouraging features of this π -model: first, for small systems it is good almost as HPHF, and, independently of the molecular size, it is simple as QCTB; second, QCLRI possesses size-consistency. Evidently, these features are indispensable for large-scale systems. Moreover, π -electron radicals and polyradicals, and related spintronics problems are attractive as well for studying by DODS, but they cannot well be handled in a too simple way. However, the ground triplet states may be easily treated approximately by the proposed HPHF methodology, and we hope to address this and other mentioned problems in a near future.

Appendices

Appendix A: Construction of HPHF Green's Function

Before treating in detail GF for HPHF, it is sensible to consider a standard general expression of GF. Let us first rewrite Eq. (22.2) in an appropriate spectral form:

$$R = \sum_i \frac{|\phi_i\rangle \langle \phi_i|}{E + i0^+ - \varepsilon_i} + \sum_a \frac{|\phi_a\rangle \langle \phi_a|}{E + i0^+ - \varepsilon_a}, \quad (22.A1)$$

where ε_i and ε_a are Koopmans orbital energies, that is eigenvalues of h ; $|\phi_i\rangle$ and $|\phi_a\rangle$ are corresponding occupied and virtual MOs (eigenkets of h), respectively. In fact, the structure of Eq. (22.A1) remains valid in a more general setting (as in Eq. (5.76) from Ref. [1]). In doing so, $|\phi_i\rangle$ and $|\phi_a\rangle$ should be replaced by the so-called Dyson orbital $|d_i^+\rangle$ for electron detachment, and by Dyson orbital $|d_a^-\rangle$ for electron attachment; they may be nonorthogonal to each other and even be linear dependent [50]. In addition, ε_i and ε_a are replaced with transition energies ΔE_i^+ and ΔE_a^- , respectively. Explicitly, $\Delta E_i^+ = E^N - E_i^{N-1}$ (negative ionization potential), and $\Delta E_a^- = E_a^{N+1} - E^N$ (electron affinity). It gives the most general (Lehmann type) spectral representation of GF for N -electron system:

$$R = \sum_i \frac{|d_i^+\rangle \langle d_i^+|}{E + i0^+ - \Delta E_i^+} + \sum_a \frac{|d_a^-\rangle \langle d_a^-|}{E + i0^+ - \Delta E_a^-}. \quad (22.A2)$$

Now we turn to the HPHF model for which the variational Koopmans-like orbitals were constructed in Ref. [28]. We will need the standard (Hermitian) matrix projectors onto the occupied spin-up and spin-down MOs, that is

$$\rho^\alpha = \sum_{i=1}^n |\phi_i^\alpha\rangle \langle \phi_i^\alpha|, \quad \rho^\beta = \sum_{i=1}^n |\phi_i^\beta\rangle \langle \phi_i^\beta|, \quad (22.A3)$$

along with a non-Hermitian matrix projector U which is generated by overlapping of ρ^α and ρ^β :

$$U = \rho^\alpha (\rho^\beta \rho^\alpha)^{-1} \rho^\beta. \quad (22.A4)$$

Matrix inversion here should be understood as the Moore-Penrose pseudoinverse (see, e.g., Ref. [51]). The next are the Fockian matrices, f_α and f_β , associated with the above projectors:

$$f_\alpha = h + J(\rho^\alpha + \rho^\beta) - K(\rho^\alpha), \quad f_\beta = h + J(\rho^\alpha + \rho^\beta) - K(\rho^\beta) \quad (22.A5)$$

$$f_U = h + J(U + U^+) - K(U), \quad (22.A6)$$

with J and K being, respectively, standard Coulomb and exchange (super)operators due to Roothaan. In above, h is a core Hamiltonian which includes not only h^0 but electron-nuclear attraction terms.

Then we can derive the HPHF variational equation for $|d_i^+\rangle$, based on Eqs. (35) and (36) from Ref. [28]. We first define the (nonnormalized) charge density matrix, D , at the HPHF level:

$$D = \rho^\alpha + \rho^\beta + \xi (U + U^+), \quad (22.A7)$$

where ξ is a pseudodeterminant of $\rho^\alpha \rho^\beta$ (i.e., the last nonnull (n th) coefficient of its characteristic polynomial). This D serves as an auxiliary matrix in the generalized eigenvalue problem of the form:

$$\Theta D^{-1} |d_i^+\rangle = (E_{\text{HPHF}} - \Delta E_i^+) |d_i^+\rangle, \quad (22.A8)$$

where

$$\Theta = \rho^\alpha (E_\rho - f_\alpha) \rho^\alpha + \rho^\beta (E_\rho - f_\beta) \rho^\beta + \xi [U (E_U - f_U) U + \text{h.c.}], \quad (22.A9)$$

and E_ρ and E_U are usual UHF-like energies for projectors ρ^α , ρ^β and U , U^+ , respectively. Moreover, E_{HPHF} (i.e., E_N needed for ΔE_i^+) is known beforehand: $E_{\text{HPHF}} = (E_\rho + \xi E_U)/(1 + \xi)$. The eigenvalue problem for $|d_a^-\rangle$ and ΔE_a^- is formulated likewise. Namely, the relevant eigenvalue problem for ΔE_a^- can be obtained from Eqs. (22.A5), (22.A6), (22.A7), (22.A8), and (22.A9) by replacing all projectors by their “vacant” counterparts ($\rho^\alpha \rightarrow I - \rho^\alpha$, $U \rightarrow I - U$ etc.), but leaving all the Fockians, Eqs. (22.A5) and (22.A6), unchanged. At last, in order to get the resulting R^{HPHF} from the eigensolutions of Eq. (22.A8) and their counterparts for ΔE_a^- , we directly apply Eq. (22.A2).

We now shortly discuss the selection rules for matrix R_0 , i.e., for GF matrix elements at $E = E_F$, neglecting energy broadening effects. The main rule is that for any correct bipartite-symmetry description we have the same block skew-diagonal structure of R_0 as in the underlying TB Hamiltonian, Eq. (22.5). Thus,

$$R_0 = \begin{pmatrix} 0 & R_{*o} \\ R_{o*} & 0 \end{pmatrix}. \quad (22.A10)$$

This equation for TB is trivial because $R_0^{\text{TB}} = -(h^0)^{-1}$. Eq. (22.A10) is indeed the selection rule since it states that there are no nonzero elements of GF for (a, b) connections with a and b belonging simultaneously to the same atomic set, either the starred or unstarred set. Far less trivial is the fact that Eq. (22.A10) holds true for GF at the π -FCI level, as was stated rigorously in the important theorem obtained in Ref. [18]. Therefore, Eq. (22.A10) as originating from the bipartite symmetry, should be valid for any consistent π -approximation not violating a topological symmetry. The

same selection is exactly fulfilled for QCTB [20], and it is not so difficult to prove the same rule at the HPHF level as well.

Appendix B: Approximate Versus “Exact” π -Electron Results for Small Aromatics

In order to estimate reliability of the results obtained by various approximate π -models, we consider briefly the formally exact π -electron theory based on the well-known FCI method (e.g., see [52]). In our computations, we will follow the previously proposed FCI matrix algorithm; for additional references see Ref. [53] where a suitable FCI approach to calculating Dyson orbitals is given. As to the MSE problems, the first important results at the π -FCI level were given only recently in Ref. [18]. In what follows, the FCI results we present here will be taken as the benchmark data against which all the others must be compared.

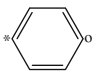
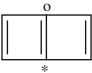
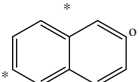
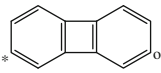
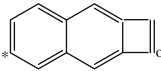
One special point concerns the actual Fermi energy E_F that should be used to ensure Eq. (22.A10) for bipartites. In Ref. [18] the E_F value is not given explicitly. At the same time, for bipartites the remarkable Hush and Pople theorem is valid at the π -electron Hartree-Fock level [54], as well as at the FCI level [55]. From this theorem it follows that $E_F = W_C + \gamma_C/2$, where W_C is the standard effective ionization potential, and γ_C is the π -electron one-center Coulomb repulsion integral for the carbon atom. Just this choice of E_F ensures the validity of Eq. (22.A10) and other properties of GF for bipartites.

In our specific π -electron computations, we use standard π -electron parameters (in eV): resonance integral of the aromatic π -bond $\beta_0 = -2.4$; $W_C = 0$, $\gamma_C = 11.13$, and two-center repulsion integrals due to Ohno. For QCTB computations, we adopt $\delta = 7/24$ and $E_F = 0$. The idealized regular geometry was taken for the carbon backbone in all studies of conjugated π -structures (1.4 Å for CC bond lengths, etc.).

Now, let us say few words about the supplementary rescaling of the GF matrix elements for RHF, HPHF, and FCI, following the procedure from Ref. [20]. This was proposed in order to avoid an inevitably large gap between different approaches. When multiplying RHF, HPHF, and FCI matrix elements of GF by the scaling factor $\beta_0/(\beta_0 - \gamma_{12}/2)$ we make them comparable with their TB and QCTB counterparts. In particular, in the ethylene molecule the respective (1,2) elements, $(R_0^{\text{TB}})_{1,2}$ and $(R_0^{\text{RHF}})_{1,2}$ for the CC π bond, become identical and equal to 1.

Now we describe the results of comparison between π -FCI (the most rigorous π -approach) and main approximations (HPHF, RHF, QCTB, and TB). In addition, we tentatively and preliminary propose an improvement of QCTB in order to include long-range interactions not incorporated in the topological schemes. We simply do the first iteration of an usual self-consistent RHF procedure based on the TB (Hückel) density matrix as a start. It gives us a modified one-electron Hamiltonian of the correct block structure as in Eq. (22.5) for h^0 . Then, expressions of the same

Table 23.3 GF matrix elements R_0 ($E = E_F$) for small aromatic molecules at the various levels of the theory

Structure	R_0^{FCI}	R_0^{HPHF}	R_0^{QCLRI}	R_0^{RHF}	R_0^{QCTB}	R_0^{TB}
	-0.447	-0.458	-0.439	-0.496	-0.451	-0.500
	-0.328	-0.374	-0.357	-0.497	-0.603	-1.000
	0.236	0.245	0.232	0.270	0.275	0.333
	-0.138	-0.139	-0.133	-0.150	-0.215	-0.333
	-0.156	-0.157	-0.164	-0.170	-0.271	-0.5

The used (*, o) connections are shown on the structural formulas

type as in Eqs. (22.7), (22.8), (22.9), and (22.10) are applied in order to compute an approximated GF. This approach will be termed the quasi-correlated long-range interaction (QCLRI) model, and the respective GF will be denoted by G^{QCLRI} . More detail will be given elsewhere.

Let us examine the numerical results presented in Table 22.3. The specific connections (*, o) are shown in Table 22.3 by stars and circles. We see that HPHF provides the best (in respect to FCI) results whereas there are marked quantitative deviations of QCTB from FCI. Especially large deviations from FCI occur for TB. It is worth paying attention to a good quality of the RHF results for the considered small aromatic molecules. In fact, RHF provides here better results than TB and even QCTB. However, RHF calls for much more computational efforts, but more essential is that RHF is not appropriate for computing GF in extended π -systems (see Sect. 22.5). It is important for future applications to observe that QCLRI, i.e., the above-proposed simple π -scheme, surprisingly works almost as well as HPHF, at least for the considered molecules. It is noteworthy that, unlike QCTB, the QCLRI method possesses the size-consistency discussed in the last paragraph of Sect. 22.4).

It is pertinent to understand now how significant in practice can be errors caused by lacking size-consistency in HPHF. A direct way to estimate actual inaccuracy due to the size inconsistency is to compute GF matrix elements in non-covalent intermolecular dimers of the chosen systems. Indeed, GF should be an additive-type size-consistent quantity (as closely related to the one-electron density matrix), and the same follows also from definition (22.A2). It means that the GF matrix of any noncovalent intermolecular dimer or complex, say, complex AB, must take the form of a direct sum when an average intermolecular distance goes to infinity. For example, in a dissociated dimer AB we have at the FCI level,

$R^{\text{FCI}}[AB] = R^{\text{FCI}}[A] \oplus R^{\text{FCI}}[B]$, and likewise for other size-consistent models, such as RHF, QCLRI, QCTB, and TB. Unfortunately, this is not the case of HPHF and related spin-projected Hartree-Fock models.

Let us examine the selected GF elements of the dimerized systems for the molecules studied in Table 22.3. For each dissociated dimer, its constituent monomeric parts A and B were situated at the intermolecular distance equal to 100 Å. Of course, FCI, QCLRI, RHF, QCTB, and TB obey the size-consistent requirement, so that the corresponding GF matrix elements in the initial monomer molecule and in the related parts of the dimer are exactly the same, and we do not repeat these data. At the same time, in the case of HPHF we obtain slightly different results for the monomer and the respective dimer subunits. We find the following HPHF values for GF elements under dissociation of the benzene, butalene, naphthalene, diphenylene, and naphtha[b]cyclobutadiene dimers:

$$-0.475, -0.407, 0.255, -0.142, -0.157$$

These values should be compared with the respective values in the third column of Table 22.3. We see that in the dissociated dimers the deviation of GF elements from the ones obtained for the monomer are around of order 5%.

References

1. Cuevas JC, Scheer E (2017) *Molecular electronics: an introduction to theory and experiment*, 2nd edn. World Scientific, Singapore
2. Solomon GC, Herrmann C, Ratner MA (2012) Molecular electronic junction transport: some pathways and some ideas. *Top Curr Chem* 313:1–38
3. Metzger RM (2015) Unimolecular electronics. *Chem Rev* 115:5056–5115
4. Moth-Poulsen K (ed) (2016) *Handbook of single-molecule electronics*. Pan Stanford Publishing Pte Ltd, Singapore
5. Xiang D, Wang X, Jia C, Lee T, Guo X (2016) Molecular-scale electronics: from concept to function. *Chem Rev* 116:4318–4440
6. Tsuji Y, Estrada E, Movassagh R, Hoffmann R (2018) Quantum interference, graphs, walks, and polynomials. *Chem Rev* 118:4887–4911
7. Ernzerhof M, Bahmann H, Goyer F, Zhuang M, Rocheleau P (2006) Electron transmission through aromatic molecules. *J Chem Theory Comput* 2:1291–1297
8. Fowler PW, Pickup BT, Todorova TZ, Myrvold W (2009) Conduction in graphenes. *J Chem Phys* 131:244110-1-8
9. Markussen T, Stadler R, Thygesen KS (2010) The relation between structure and quantum interference in single molecule junctions. *Nano Lett* 10:4260–4265
10. Pedersen KGL, Borges A, Hedegård P, Solomon GC, Strange M (2015) Illusory connection between cross-conjugation and quantum interference. *J Phys Chem C* 119:26919–26924
11. Tsuji Y, Hoffmann R, Movassagh R, Datta S (2014) Quantum interference in polyenes. *J Chem Phys* 141:224311-1-13
12. Markussen T, Stadler R, Thygesen KS (2011) Graphical prediction of quantum interference-induced transmission nodes in functionalized organic molecules. *Phys Chem Chem Phys* 13:14311–14317

13. Wang X, Spataru CD, Hybertsen MS, Millis AJ (2008) Electronic correlation in nanoscale junctions: comparison of the GW approximation to a numerically exact solution of the single-impurity Anderson model. *Phys Rev B* 77:045119-1-10
14. Bergfield JP, Stafford CA (2009) Many-body theory of electronic transport in single-molecule heterojunctions. *Phys Rev B* 79:245125-1-10
15. Yeriskin I, McDermott S, Bartlett RJ, Fagas G, Greer JC (2010) Electronegativity and electron currents in molecular tunnel junctions. *J Phys Chem C* 114:20564–20568
16. Bergfield JP, Solomon GC, Stafford CA, Ratner MA (2011) Novel quantum interference effects in transport through molecular radicals. *Nano Lett* 11:2759–2764
17. Goyer F, Ernzerhof M (2011) Correlation effects in molecular conductors. *J Chem Phys* 134:174101-1-10
18. Pedersen KGL, Strange M, Leijnse M, Hedegard P, Solomon GC, Paaske J (2014) Quantum interference in off-resonant transport through single molecules. *Phys Rev B* 90:125413-1-11
19. Hoy EP, Mazziotti DA, Seideman T (2017) Development and application of a 2-electron reduced density matrix approach to electron transport via molecular junctions. *J Chem Phys* 147:184110-1-8
20. Luzanov AV (2019) Single-molecule electronic materials: conductance of π -conjugated oligomers within quasi-correlated tight-binding model. *Funct. Mater* 26:152–163
21. Luzanov AV (2014) Effectively unpaired electrons in bipartite lattices within the generalized tight-binding approximation: application to graphene nanoflakes. *Funct Mater* 21:437–447
22. Luzanov AV (2016) Effectively unpaired electrons for singlet states: from diatomics to graphene nanoclusters. In: Leszczynski J, Shukla MK (eds) *Practical aspects of computational chemistry IV*. Springer, Boston, pp 151–206
23. Luzanov AV, Plasser F, Das A, Lischka H (2017) Evaluation of the quasi correlated tight-binding (QCTB) model for describing polyradical character in polycyclic hydrocarbons. *J Chem Phys* 146:064106-1-12
24. Davison SG, Amos AT (1965) Spin polarized orbitals for localized states in crystals. *J Chem Phys* 43:2223–2233
25. Estrada E (2018) The electron density function of the Hückel (tight-binding) model. *Proc R Soc A* 474:20170721-1-18
26. Smeyers YG, Doreste-Suarez L (1973) Half-projected and projected Hartree-Fock calculations for singlet ground states. I. Four-electron atomic systems. *Int J Quantum Chem* 7:687–698
27. Cox PA, Wood MN (1976) The half-projected Hartree-Fock method. I. Eigenvalue formulation and simple application. *Theor Chim Acta* 41:269–278
28. Luzanov AV (1985) The spin-symmetrized Hartree-Fock method. *J Struct Chem* 25:837–844
29. Bone RGA, Pulay P (1992) Half-projected Hartree-Fock natural orbitals for defining CAS–SCF active spaces. *Int J Quant Chem* 45:133–166
30. Smeyers YG (2000) The half projected Hartree-Fock model for determining singlet excited states. *Adv Quant Chem* 36:253–270
31. Verzijl CJO, Seldenthuis JS, Thijssen JM (2013) Applicability of the wide-band limit in DFT-based molecular transport calculations. *J Chem Phys* 138:094102-1-10
32. Jhan S-M, Jin B-Y (2017) A simple molecular orbital treatment of current distributions in quantum transport through molecular junctions. *J Chem Phys* 147:194106-1-10
33. Langer W, Plischke M, Mattis D (1969) Existence of two phase transitions in Hubbard model. *Phys Rev Lett* 23:1448–1452
34. Langer W, Mattis D (1971) Ground state energy of Hubbard model. *Phys Lett A* 3:139–140
35. Tyutyulkov N (1975) A generalized formula for the energies of alternant molecular orbitals. I. Homonuclear molecules. *I J Quantum Chem* 9:683–68936
36. Löwdin P-O (1955) Quantum theory of many-particle systems. III. Extension of the Hartree-Fock scheme to include degenerate systems and correlation effects. *Phys Rev* 97:1505–1520
37. Waller I, Hartree DR (1929) On the intensity of total scattering of X-rays. *Proc R Soc London A* 124:119–142
38. Lyakh DI, Musiał M, Lotrich VF, Bartlett RJ (2011) Multireference nature of chemistry: the coupled-cluster view. *Chem Rev* 112:182–243

39. Tada T, Yoshizawa K (2002) Quantum transport effects in nanosized graphite sheets. *Chem Phys Chem* 3:1035–1037
40. Morikawa T, Narita S, Klein DJ (2005) Molecular electric conductance and long-bond structure counting for conjugated-carbon nano-structures. *Chem Phys Lett* 402:554–558
41. Schomerus H (2007) Effective contact model for transport through weakly-doped graphene. *Phys Rev B* 76:045433-1-7
42. Cuansing E, Wang JS (2009) Quantum transport in honeycomb lattice ribbons with armchair and zigzag edges coupled to semi-infinite linear chain leads. *Euro Phys J B* 69:505–513
43. Nelson T, Zhang B, Prezhdov OV (2010) Detection of Nucleic Acids with Graphene Nanopores: Ab Initio Characterization of a Novel Sequencing Device. *Nano Lett* 10:3237–3242
44. Rangel NL, Leon-Plata PA, Seminario JM (2012) Computational Molecular Engineering for Nanodevices and Nanosystems. In: Leszczynski J, Shukla MK (eds) *Practical aspects of computational chemistry I*. Springer, Heidelberg, pp 347–383
45. Qiu W, Skafidas E (2013) Quantum conductance of armchair graphene nanopores with edge impurities. *J Chem Phys*: 114: 073703–073701–8
46. Güçlü AD, Potasz P, Korkusinski M, Hawrylak P (2014) *Graphene Quantum Dots*. Springer, Berlin/Heidelberg/New York
47. Luzanov A (2018) Graphene Quantum Dots in Various Many-Electron π -Models. In: Fesenko O, Yatsenko L (eds) *Nanophysics, nanophotonics, and applications*. Springer proceedings in physics, vol 210. Springer, Cham, pp 161–174
48. Peng J, Gao W, Gupta BK, Liu Z, Romero-Aburto R, Ge L, Song L, Alemany LB, Zhan X, Gao G, Vithayathil SA, Kaiparettu BA, Marti AA, Hayashi T, Zhu JJ, Ajayan PM (2012) Graphene quantum dots derived from carbon fibers. *Nano Lett* 12:844–849
49. McWeeny R (1992) *Methods of molecular quantum mechanics*. Academic Press, London
50. Goscinski O, Lindner P (2003) Natural spin-orbitals and generalized overlap amplitudes. *J Math Phys* 11:1313–1317
51. Albert AE (1972) *Regression and the Moore-Penrose pseudoinverse*. Academic Press, New York
52. Amos AT, Woodward M (1969) Configuration-interaction wavefunctions for small pi systems. *J Chem Phys* 50:119–123
53. Luzanov AV, Ivanov VV, Boichenko IV (1996) Semiempirical determination of Dyson's states in conjugated systems within a full-CI π -electron scheme. *J Mol Struct (THEOCHEM)* 360:167–174
54. Pople JA, Hush NS (1955) Ionization potentials and electron affinities of conjugated hydrocarbon molecules and radicals. *Trans Faraday Soc* 51:600–605
55. McLachlan AD (1959) The pairing of electronic states in alternant hydrocarbons. *Mol Phys* 2:271–284